Molecular Quantum Rings Formed from a π-Conjugated Macrocycle

Chris J. Judd[1], Anton S. Nizovtsev,[2,3,4] Rikke Plougmann[1], Dmitry V. Kondratuk,[5] Harry L. Anderson,[5]
Elena Besley[2,*] and Alex Saywell[1,†]

[1]*School of Physics & Astronomy, The University of Nottingham, Nottingham NG7 2RD, United Kingdom*
[2]*School of Chemistry, The University of Nottingham, Nottingham NG7 2RD, United Kingdom*
[3]*Nikolaev Institute of Inorganic Chemistry, Siberian Branch of the Russian Academy of Sciences,*
Academician Lavrentiev Avenue 3, 630090 Novosibirsk, Russian Federation
[4]*Novosibirsk State University, Pirogova Street 2, 630090 Novosibirsk, Russian Federation*
[5]*Department of Chemistry, University of Oxford, Oxford OX1 3TA, United Kingdom*

The electronic structure of a molecular quantum ring (stacks of 40-unit cyclic porphyrin polymers) is characterized via scanning tunneling microscopy and scanning tunneling spectroscopy. Our measurements access the energetic and spatial distribution of the electronic states and, utilizing a combination of density functional theory and tight-binding calculations, we interpret the experimentally obtained electronic structure in terms of coherent quantum states confined around the circumference of the π-conjugated macrocycle. These findings demonstrate that large (53 nm circumference) cyclic porphyrin polymers have the potential to act as molecular quantum rings.

Quantum rings are structures that facilitate phase-coherent electron motion around a closed path and exhibit quantum phenomena, including the Aharonov-Bohm effect [1] and persistent currents [2–4]. Although ring structures may be fabricated from semiconducting materials, e.g., thermal conversion of InAs quantum dots [5,6], this approach leads to significant variation in the size and morphology of the rings [7,8], likely to give rise to inhomogeneous broadening and shifting of energy levels [9,10]. An alternative approach whereby quantum rings are engineered by atomic manipulation (utilizing a scanning tunneling microscope to sequentially move individual atoms) has been shown to provide well-defined periodic potentials and corresponding quantized energy levels [11], although this type of "bottom-up" fabrication is not only inherently labor intensive but extremely difficult to scale up. In addition, the electronic structure of on-surface synthesized molecular rings has been studied [12], successfully modeling electronic confinement within a two-dimensional ribbon adsorbed upon a metal surface.

Our approach is to utilize cyclic porphyrin polymers as molecular quantum rings. These cyclic polymers possess a delocalized π-conjugated electronic structure and have been shown to exhibit ring currents for systems containing up to 12 porphyrin subunits (16 nm circumference) [13,14]. Using a Vernier templating method [15], rings containing a range of porphyrin units (5–50) may be produced [16–18]. Here we employ a combination of scanning tunneling microscopy (STM) and scanning tunneling spectroscopy (STS) to access the energy and spatial position of the electronic states of a 40 unit cyclic porphyrin polymer within stacks of 2–3 rings supported on a Ag(111) substrate. Our experimental results are compared with density-functional theory (DFT) and extended tight-binding (GFN1-XTB method [19]) calculations, which indicate that the electronic states of the porphyrin rings within the stacks are similar to those of an isolated ring, and that the spatial distribution of the observed states is a consequence of coherent quantum confinement within the molecular quantum ring.

The structure of the cyclic porphyrin nanoring (*c*-P40) studied here is shown in Fig. 1(a). Each nanoring consists of 40 Zn-porphyrin units covalently bonded via butadiyne linkers to form a cyclic polymer [variant used within these experiments is functionalized with two 3,5-bis(octyloxy) phenyl side groups (Ar_1), calculations performed with truncated alkyl chains (Ar_2)]. Stacks of *c*-P40 nanorings (typically 2–3 rings) were transferred from solution, via electrospray deposition, to a Ag(111) surface held under vacuum (UHV) conditions, using a previously reported procedure [20,21]. The resulting structures are characterized by STM with the substrate held under UHV at cryogenic temperatures ($\sim$78 K).

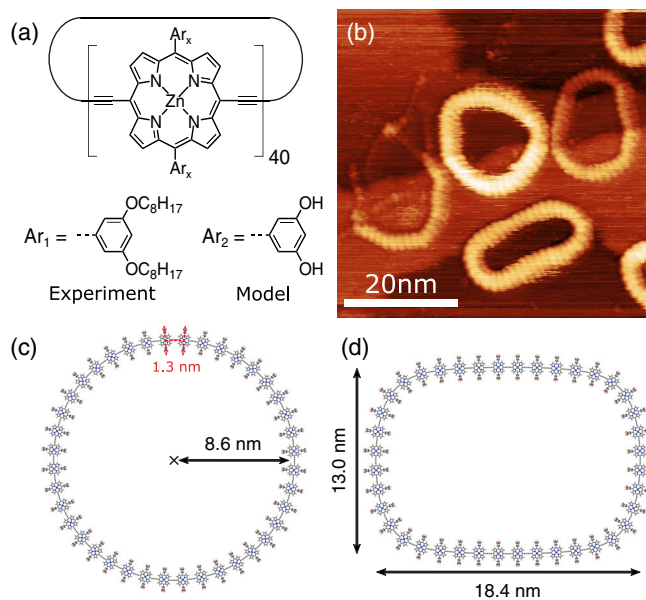The STM topograph presented in Fig. 1(b) shows stacked *c*-P40 rings on Ag(111) acquired in constant-current mode.

FIG. 1.   (a) Chemical structure of c-P40. (b) STM image of c-P40 nanoring stacks on Ag(111). Individual porphyrin units are resolved ($I_{set} = 10$ pA, $V = -1.8$ V). (c) Energy minimized structure of c-P40 model and (d) structure of c-P40 constrained to average experimental dimensions, calculated using an extended tight-binding approach.

FIG. 2.   (a) Calculated energies of occupied and unoccupied orbitals for linear porphyrin chains (l-PN, N = 1–7) and c-P40 calculated with XTB and DFT methods (see legend) (eigenvalue and ΔSCF techniques used to calculate HOMO-LUMO and −IP and −EA values, respectively). Exponential curves fitted using l-PN, N = 1–7 and extrapolated values for c-P40 based upon DFT are shown. Break in x axis after l-P7 included for clarity, see Supplemental Material [21] for full graphs. (b) Molecular orbital structures calculated for l-P7.

The stacked nanorings are observed in a variety of non-circular geometries (due to the flexibility of the rings [17]), and the different contrasts observed indicates variation in the number of rings within the stack [32] [a broken c-P40 ring to the upper left of the image exhibits image contrast comparable to that of an unstacked polymer on the Ag(111) surface].

The optimized structure of a single circular c-P40 molecule, calculated through an XTB approach [21], is shown in Fig. 1(c) with the calculated diameter of the ring and separation between porphyrin units indicated (in good agreement with previous experimental observations [33]). In addition, an optimized structure using starting conditions based on the average dimensions of experimentally observed rings is shown in Fig. 1(d). The small difference in energy between the structures [$\Delta E = 0.15$ eV, structure shown in Fig. 1(c) is more favorable] accounts for the range of ring conformations observed in the STM data.

Our discussion of the electronic properties of c-P40 is underpinned by calculations of the energy levels of unoccupied and occupied orbitals and the spatial distribution of these states. The computational expense to calculate energy levels and molecular orbitals using DFT for the c-P40 structure is prohibitive and we therefore employ a semiempirical approach based on the GFN1-XTB method [14] for the complete ring. However, we start by demonstrating the validity of our computational approach by comparing short linear chains of porphyrins investigated by XTB and DFT levels of theory (details in the Supplemental
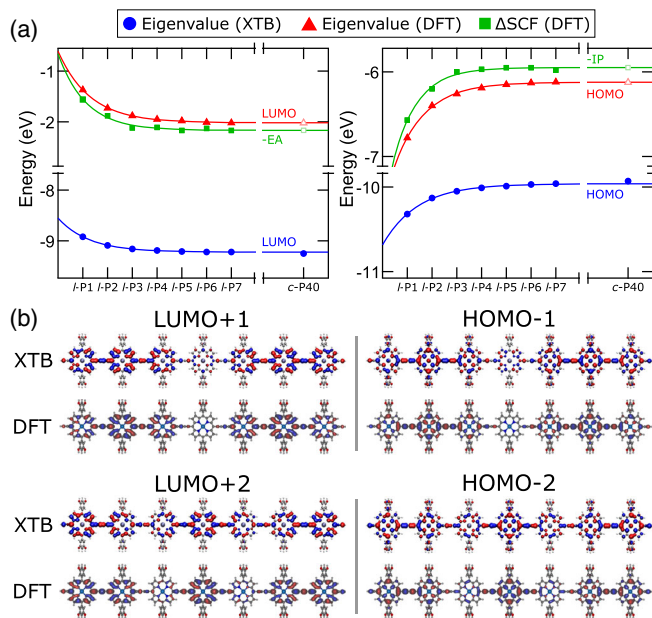
Material [21]). The highest (lowest) lying occupied (unoccupied) electronic orbitals were calculated for linear porphyrin chains consisting of N monomer units (l-PN, N = 1–7) using both XTB and DFT methods [Fig. 2(a)]. We have also investigated the use of the Δ self-consistent field (ΔSCF) technique to calculate the ionization potential (IP) and electron affinity (EA) of the compounds under study (these values can be compared to experimentally measured quantities [34]). From Fig. 2(a) it can be seen that, irrespective of the level of theory applied, the energy for all states converges as the length of the polymer chain is increased (l-P1 − l-P7). We have modeled this convergence as an exponential dependence and the phenomenological model shows good agreement with data.

In the case of the XTB approach, we may directly compare the extrapolated value for an l-P40 chain to that calculated for the c-P40 ring. The high level of agreement [e.g., −9.93 eV compared with −9.96 eV from the extrapolated value for the highest occupied molecular orbital (HOMO) energy] allows us to perform a similar extrapolation, based upon the DFT calculations for the chains l-P1–l-P7, to obtain values for the c-P40 ring [see Fig. 2(a)]. Although good agreement is found for extrapolated HOMO and lowest unoccupied molecular orbital (LUMO) values, deviation occurs for higher and lower lying states.

We also compare the spatial distribution of molecular orbitals for l-PN ($N = 1$–7) as calculated by XTB and DFT methods [details of the l-P7 chain are shown in Fig. 2(b)]. It is evident that there is good agreement with respect to the spatial position of the two orbitals immediately above the LUMO and below the HOMO. Both theoretical protocols predict a similar shape to the molecular orbitals, showing the same spatial distribution of localized clusters of higher electron density, which match qualitatively with the expected solutions to electron confinement within a 1D potential well. The equivalence of these results indicates that XTB is a suitable method for the qualitative analysis of the electronic structure of large c-P40 nanorings.

STS was subsequently used to gain insight into the electronic structure and molecular orbitals of stacked c-P40 rings. In this technique, differential conductance (dI/dV) is measured as a function of applied sample bias, with the tip held fixed at a specific point [35]. Conductance spectra were acquired using a lock-in technique (rms bias modulation of 10 mV). The acquired differential conductance is proportional to the density of states at that location and hence provides information on the energies at which resonant tunneling occurs (attributed to electronic states present at that location).

STS spectra were obtained for a number of locations above stacks of c-P40 (>200 spectra acquired [21]). An example spectrum is shown in Fig. 3(a), acquired on a nanoring at the position indicated in Fig. 3(b) (the STS data

for the substrate are presented in the Supplemental Material [21]). Three distinct electronic resonances are observed in the spectrum. Those at approximately -1.0 and 0.70 V, are labeled R_0 and R_1, respectively, with the additional higher energy resonance at 1.1 V being labeled R_2. Our interpretation of the observed resonances is based upon a comparison with the DFT-calculated ionization potentials, discussed above, and previously reported optical transitions of linear and cyclic porphyrin polymers [36–38].

In Fig. 3(c) we present DFT-based ionization potentials and electron affinities for l-P1–l-P7 and c-P40. Also included are two datasets showing the predicted excited state energies of the c-P40 structure based upon the calculated IP and literature values for optical transitions (E_{opt}): i.e., Q_x (~820 nm, 1.51 ± 0.08 eV) and Q_y (~580 nm, 2.14 ± 0.07 eV) bands for c-P40—see Refs. [37,38] and Table S1 in the Supplemental Material (Q_x and Q_y transitions represent, respectively, Q transitions polarized parallel and perpendicular to the $C = C$ axis of the ring [39]). A similar approach has been implemented for STS-based analysis of oligoacenes [34]. Finally, the positions of the experimentally determined tunneling resonances (R_0, R_1, and R_2) are referenced to the work function of Ag(111) (4.74 eV [40]).

We find good agreement when comparing the expected separation between Q_x and Q_y bands (0.63 ± 0.11 eV) and the measured gap between the R_1 and R_2 resonances (equivalent to 0.40 ± 0.14 eV). In addition, the measured separation between R_0 and R_1 (1.70 ± 0.18 eV) matches the Q_x transition (1.51 ± 0.08 eV). The data presented in Fig. 3(c) demonstrate alignment between the DFT-calculated ionization potential of c-P40 and the experimentally observed electronic tunneling resonance R_0, indicating that R_0 is associated with the electronic ground state of the molecular rings. The observation that the R_1 resonance does not agree with the calculated EA has been previously observed for related systems [34] and may be attributed to the transient population of an excited state during tunneling resonance, as opposed to the creation of a negative charged species in the case of EA. However, one may interpret the resonances R_1 and R_2 by considering $-$IP$ + E_{opt}$; with R_2 corresponding to the Q_y transition [cf. $R_2 = -3.64 \pm 0.14$ and $-$IP$ + E_{opt}(Q_y) = -3.81 \pm 0.07$ eV] and R_1 assigned to the Q_x transition (the intrinsic flexibility of c-P40 will introduce variation in Q_x and Q_y [36], which may account for discrepancies between R_1 and the Q_x transition).

To study the spatial distribution of molecular states at various energies (including resonant features R_0, R_1, and R_2) differential conductance maps, recorded over a range of sample biases, were acquired for several stacks of c-P40 nanorings. Figure 4 shows conductance maps of a single stack of rings on a flat area (acquired at $+1.3 \rightarrow -1.3$ V). In general, greater intensity is seen in images with biases in the ranges of $-0.9 \rightarrow -1.0$ and $0.7 \rightarrow 0.9$ V
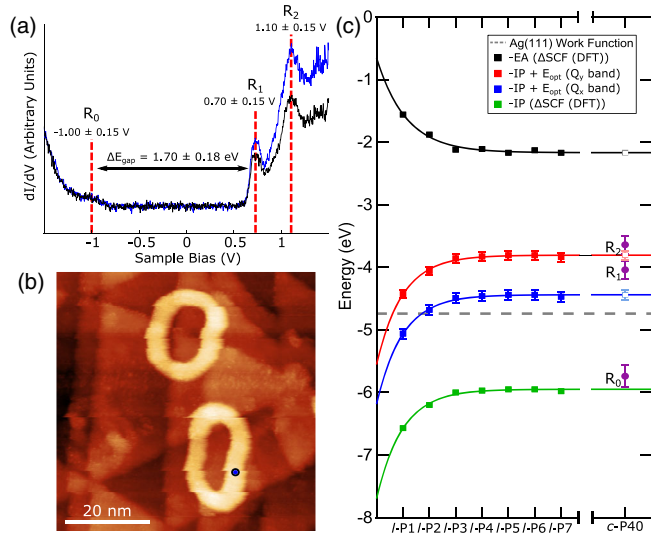

FIG. 3. (a) Example forward (blue) and reverse (black) STS spectrum showing differential conductance as a function of applied sample bias. (b) STM image showing spectroscopy location (blue dot). Discontinuities in image occur due to thermal drift between spectra ($I_{set} = 40$ pA, $V = 1.5$ V). (c) Energy levels as a function of polymer length (DFT calculations, see legend). Experimentally determined values for electronic resonances R_0, R_1, and R_2 are shown. STM image and spectrum acquired at ~78 K.
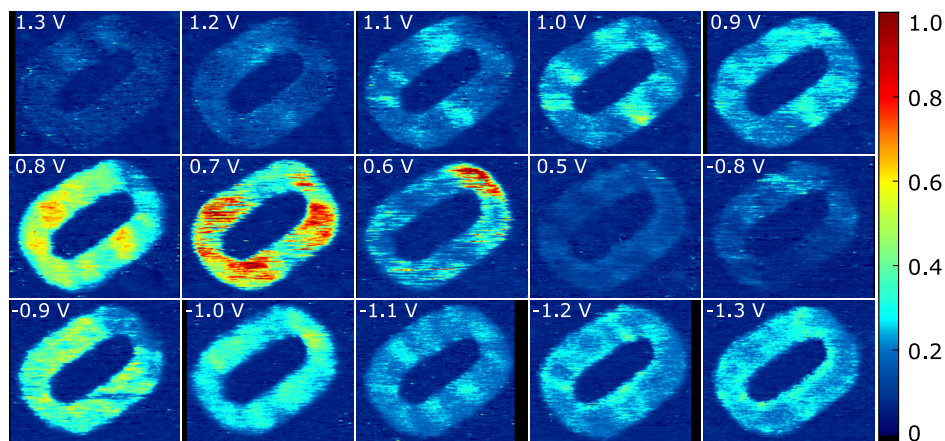
FIG. 4. Differential conductance maps for a c-P40 nanoring stack acquired at sample bias $+1.3$ to -1.3 V (intensity normalized to maximum measured dI/dV across all images). Color scale shows normalized differential tunneling conductance ($I_{set} = 40$ pA, image dimensions 28.4×23.5 nm). Bright contrast features occur at bias values matching observed resonances in dI/dV spectra. Bright stripe features visible for several biases.

[corresponding to electronic resonances R_0 and R_1, observed in STS spectra; Fig. 3(a)]. For conductance maps acquired with an applied bias of -0.9 and -1.0 V (corresponding to $\sim R_0$), the distribution of electronic structure is delocalized and, although a variation in intensity is observed, there is no obvious periodic structure (we relate this to a dominant contribution from the HOMO of c-P40, shown in Fig. S7 [21]). Increasing the sample bias to -1.1 V, allowing access to additional occupied states, results in the observation of a regular arrangement of "stripe" features around the rings (qualitatively similar to that expected for coherent electronic states confined within a conducting quantum ring).

Focusing on conductance maps acquired at resonances R_1 and R_2 ($+0.7$ and $+1.1$ V, respectively), the images show regions of higher and lower intensity around the rings producing aperiodic bands. As our XTB calculations predict a very small difference in energy between molecular orbitals (e.g., <10 meV, see Table S2 [21]), and as the energy resolution of the dI/dV maps is limited to ±14 mV, the acquired conductance maps are likely to be a convolution of several molecular orbitals within this energy range. In addition, one should note that the broad resonances (corresponding to the known optical transitions) are expected to encompass several molecular orbital states. As such, the features observed will (i) be a convolution of several structures and (ii) may exhibit a majority contribution from a particular state, depending on relative strengths of the tunneling probabilities. The conductance map associated with R_1 is relatively diffuse (likely to indicate a contribution from the LUMO and some higher lying unoccupied molecular orbitals). For the R_2 resonance, the conductance maps show the appearance of banded structures, potentially indicating a contribution from a range of LUMO $+N$ orbitals.

It is important to consider the expected separation between energy levels for quantum rings and the

relationship with the observed resonances in the STS spectra. The XTB-calculated energies for c-P40 nanorings indicate a linear dispersion relationship for states around the HOMO and LUMO (i.e., equally spaced in energy). This is in agreement with dI/dV measurements for linear oligothiophene molecular systems [41], although in contrast to that observed for hexagonal structures formed from metal adatoms [11] and small molecular rings [12]. The origin of the apparent discrepancy may be due to the interaction with the metal substrate, with the c-P40 ring stacks and oligothiophene [supported on a NaCl/Cu(111) surface [41]] both likely to be at least partially decoupled from the metallic surface states.

Returning to the spatial distribution of the bright stripe features observed at -1.1 V, Fig. 5(a) shows a differential conductance map of the same ring as shown in Fig. 4: location and separation of each stripe feature is indicated. At this energy, we observe nine stripes with an average separation of 5.8 ± 0.2 nm. These features can be
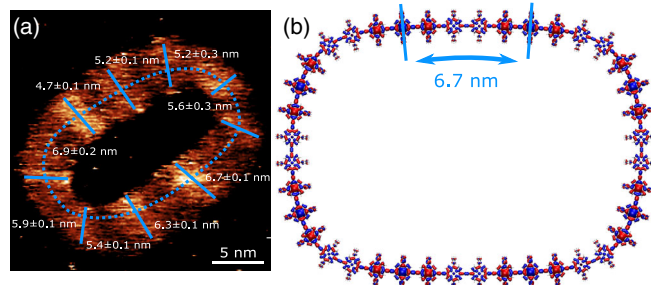

FIG. 5. Comparisons of stripe features observed in computational models and experiment. (a) Conductance map acquired at -1.1 V showing stripe features; positions and separations indicated ($I_{set} = 40$ pA). (b) Model of c-P40 HOMO-8 energy level (XTB), showing areas of high electron density separated by 6.7 nm.

compared to the XTB model of a nanoring with similar dimensions, where a spatially varying electron density is also observed, Fig. 5(b). The periodic features observed in the experimental data will contain a contribution from several occupied states (the dI/dV image at -1.1 V is acquired at 100 mV below the experimentally determined HOMO, which, based on the XTB calculations, would result in contributions from occupied states around the HOMO-8; see Table S2 [21]). Therefore, it is expected that the spatial distribution of the electron density related to all accessible energy levels should be visible [see Fig. 5(b)], with the intensity observed in the image weighted due to the electron-tunneling transition probability. These nodal structures have been absent from related studies of the electronic structure of less eccentric rings, where there is likely to be no "privileged phase origin" [12], but the noncircular geometry of the c-P40 rings may facilitate a reduction in symmetry that facilitates the observed nonuniform spatial distribution of electrons.

Based upon the separation between the stripes in the dI/dV image in Fig. 5(b), we find qualitative agreement with the calculated structure of the HOMO-8, where eight regions of higher electron density are observed with a separation of 6.7 nm. Such a finding indicates a contribution from the HOMO-8 state. However, it should be noted that the intensity of the "bands" is nonuniform, denoted by the variation in contrast within Fig. 5(a), in agreement with our assertion that we observe a convolution of electronic states. The relative contributions from different states will depend upon both the local density of states at a given energy and the tunnel barrier (which will increase for states further away from the Fermi level). It is important to note that such features (irrespective of the electronic state from which they originate) are a characteristic of a coherent electron state, which is delocalized around the c-P40 nanoring.

In summary, we have experimentally shown by a combination of STM and STS that stacks of conjugated porphyrin polymers supported on a Ag(111) surface possess quantized states and that these states are coherent around the ring with well-defined spatial distributions. These findings are supported by DFT and XTB calculations in combination with literature values of optical band gaps for these systems. This is the first demonstration of the characterization of the spatial and energetic electronic structure of such porphyrin rings, which have the potential to act as molecular quantum rings. Tuning the properties of these rings may be facilitated in future work by altering their chemical composition (e.g., varying the metallic species within the macrocycle) or their size and structure in order to provide customizable quantum molecular rings.

The experimental data on which this work is based may be found in [42].

[*]Corresponding author.
 Elena.Besley@nottingham.ac.uk
[†]Corresponding author.
 Alex.Saywell@nottingham.ac.uk

[1] M. D. Teodoro, V. L. Campo, Jr., V. Lopez-Richard, E. Marega, Jr., G. E. Marques, Y. Galvão Gobato, F. Iikawa, M. J. S. P. Brasil, Z. Y. AbuWaar, V. G. Dorogan, Yu. I. Mazur, M. Benamara, and G. J. Salamo, Phys. Rev. Lett. 104, 086401 (2010).

[2] A. C. Bleszynski-Jayich, W. E. Shanks, B. Peaudecerf, E. Ginossar, F. von Oppen, L. Glazman, and J. G. E. Harris, Science 326, 272 (2009).

[3] M. Büttiker, Y. Imry, and R. Landauer, Phys. Lett. A 96, 365 (1983).

[4] L. P. Lévy, G. Dolan, J. Dunsmuir, and H. Bouchiat, Phys. Rev. Lett. 64, 2074 (1990).

[5] A. Lorke, R. J. Luyken, A. O. Govorov, J. P. Kotthaus, J. M. Garcia, and P. M. Petroff, Phys. Rev. Lett. 84, 2223 (2000).

[6] W. Lei, C. Notthoff, A. Lorke, D. Reuter, and A. D. Wieck, Appl. Phys. Lett. 96, 033111 (2010).

[7] P. Offermans, P. M. Koenraad, J. H. Wolter, D. Granados, J. M. García, V. M. Fomin, V. N. Gladilin, and J. T. Devreese, Appl. Phys. Lett. 87, 131902 (2005).

[8] R. Timm, A. Lenz, H. Eisele, L. Ivanova, M. Dähne, G. Balakrishnan, D. L. Huffaker, I. Farrer, and D. A. Ritchie, J. Vac. Sci. Technol. B 26, 1492 (2008).

[9] J. A. Vinasco, A. Radu, E. Kasapoglu, R. L. Restrepo, A. L. Morales, E. Feddi, M. E. Mora-Ramos, and C. A. Duque, Sci. Rep. 8, 13299 (2018).

[10] O. Voskoboynikov, Y. Li, H.-M. Lu, C.-F. Shih, and C. P. Lee, Phys. Rev. B 66, 155306 (2002).

[11] V. D. Pham, K. Kanisawa, and S. Fölsch, Phys. Rev. Lett. 123, 066801 (2019).

[12] G. Reecht, H. Bulou, F. Scheurer, V. Speisser, B. Carrière, F. Mathevet, and G. Schull, Phys. Rev. Lett. 110, 056802 (2013).

[13] M. D. Peeks, T. D. W. Claridge, and H. L. Anderson, Nature (London) 541, 200 (2017).

[14] M. Rickhaus, M. Jirasek, L. Tejerina, H. Gotfredsen, M. D. Peeks, R. Haver, H.-W. Jiang, T. D. W. Claridge, and H. L. Anderson, Nat. Chem. 12, 236 (2020).

[15] M. C. O'Sullivan, J. K. Sprafke, D. V. Kondratuk, C. Rinfray, T. D. W. Claridge, A. Saywell, M. O. Blunt, J. N.

O'Shea, P. H. Beton, M. Malfois, and H. L. Anderson, Nature (London) **469,** 72 (2011).

[16] D. V. Kondratuk, J. K. Sprafke, M. C. O'Sullivan, L. M. A. Perdigao, A. Saywell, M. Malfois, J. N. O'Shea, P. H. Beton, A. L. Thompson, and H. L. Anderson, Chem. Eur. J. **20,** 12826 (2014).

[17] D. V. Kondratuk, L. M. A. Perdigão, A. M. S. Esmail, J. N. O'Shea, P. H. Beton, and H. L. Anderson, Nat. Chem. **7,** 317 (2015).

[18] P. S. Bols and H. L. Anderson, Acc. Chem. Res. **51,** 2083 (2018).

[19] S. Grimme, C. Bannwarth, and P. Shushkov, J. Chem. Theory Comput. **13,** 1989 (2017).

[20] C. J. Judd, D. V. Kondratuk, H. L. Anderson, and A. Saywell, Sci. Rep. **9,** 9352 (2019).

[21] See Supplemental Material at http://link.aps.org/supplemental/10.1103/PhysRevLett.125.206803 for experimental details and Figs. S1–S8, which includes Refs. [22–31].

[22] D. Nečas and P. Klapetek, Open Phys. **10,** 181 (2011).

[23] Y.-S. Lin, G.-D. Li, S.-P. Mao, and J.-D. Chai, J. Chem. Theory Comput. **9,** 263 (2013).

[24] F. Weigend and R. Ahlrichs, Phys. Chem. Chem. Phys. **7,** 3297 (2005).

[25] F. Weigend, Phys. Chem. Chem. Phys. **8,** 1057 (2006).

[26] S. Grimme, J. Antony, S. Ehrlich, and H. Krieg, J. Chem. Phys. **132,** 154104 (2010).

[27] S. Grimme, S. Ehrlich, and L. Goerigk, J. Comput. Chem. **32,** 1456 (2011).

[28] F. Neese, J. Am. Chem. Soc. **128,** 10213 (2006).

[29] F. Neese, F. Wennmohs, A. Hansen, and U. Becker, Chem. Phys. **356,** 98 (2009).

[30] R. Izsák and F. Neese, J. Chem. Phys. **135,** 144105 (2011).

[31] F. Neese, Comput. Mol. Sci. **8,** e1327 (2018).

[32] S. A. Svatek, L. M. A. Perdigão, A. Stannard, M. B. Wieland, D. V. Kondratuk, H. L. Anderson, J. N. O'Shea, and P. H. Beton, Nano Lett. **13,** 3391 (2013).

[33] A. Saywell, J. K. Sprafke, L. J. Esdaile, A. J. Britton, A. Rienzo, H. L. Anderson, J. N. O'Shea, and P. H. Beton, Angew. Chem. Int. Ed. **49,** 9136 (2010).

[34] F. Eisenhut, T. Kühne, F. García, S. Fernández, E. Guitián, D. Pérez, G. Trinquier, G. Cuniberti, C. Joachim, D. Peña, and F. Moresco, ACS Nano **14,** 1011 (2020).

[35] R. Wiesendanger, *Scanning Probe Microscopy and Spectroscopy: Methods and Applications* (Cambridge University Press, Cambridge, England, 1994), https://doi.org/10.1017/CBO9780511524356.

[36] M. Rickhaus, A. Vargas Jentzsch, L. Tejerina, I. Grübner, M. Jirasek, T. D. W. Claridge, and H. L. Anderson, J. Am. Chem. Soc. **139,** 16502 (2017).

[37] P. Parkinson, D. V. Kondratuk, C. Menelaou, J. Q. Gong, H. L. Anderson, and L. M. Herz, J. Phys. Chem. Lett. **5,** 4356 (2014).

[38] C.-K. Yong, P. Parkinson, D. V. Kondratuk, W.-H. Chen, A. Stannard, A. Summerfield, J. K. Sprafke, M. C. O'Sullivan, P. H. Beton, H. L. Anderson, and L. M. Herz, Chem. Sci. **6,** 181 (2015).

[39] M. Drobizhev, Y. Stepanenko, Y. Dzenis, A. Karotki, A. Rebane, P. N. Taylor, and H. L. Anderson, J. Phys. Chem. B **109,** 7223 (2005).

[40] J. Hölz and F. K. Schulte, in *Solid Suface Physics*, Springer Tracts in Modern Physics, Vol. 85 (Springer-Verlag, Berlin, 1979).

[41] J. Repp, P. Liljeroth, and G. Meyer, Nat. Phys. **6,** 975 (2010).

[42] C. J. Judd and A. Saywell, Nottingham Research Data Management Repository (2020), https://doi.org/10.17639/nott.7077.